

# Electrostatic Energy Harvester and Li-Ion Charger Circuit for Micro-Scale Applications

Erick O. Torres, *Student Member, IEEE*, and Gabriel A. Rincón-Mora, *Senior Member, IEEE*

Georgia Tech Analog and Power IC Design Lab

E-mail: ertorres@ece.gatech.edu, rincon-mora@ieee.org

**Abstract**—Modern portable micro-systems like biomedical implants and ad-hoc wireless transceiver micro-sensors continue to integrate more functions into smaller devices, which result in low energy levels and short operational lives. Researchers and industry alike are consequently considering harvesting energy from the surrounding environment as a means of offsetting this energy deficit. Even with power efficient designs, low duty-cycle operation, smart power-aware network architectures, and batteries with improved energy density, the stored energy in micro-scale systems is simply not sufficient to sustain extended lifetimes. Fortunately, the surrounding environment is a rich source of energy, from solar and thermal to kinetic, but harnessing it without dissipating much power in the process is challenging. In this paper, an electrostatic vibrational energy harvester circuit is proposed and evaluated. It harnesses energy from inherent vibrations in the system (e.g., engine-powered applications) by modulating the parallel-plate distance of a variable capacitor and channeling the resulting change in charge into a secondary Li-Ion micro-battery. The varactor, in essence, behaves like a vibration-dependent current source. Simulations show that a 100-to-1 pF variable plate capacitor subjected to vibrations with a period of 15  $\mu$ s produces an average harvesting current of 40.8  $\mu$ A, an energy gain of 569 pJ per cycle, and a net average power gain of 38  $\mu$ W.

**Keywords** – Energy harvesting, electrostatic vibration harvester circuit, lithium-ion charger, self-powered, self-sufficient, self-sustaining

## I. INTRODUCTION

Self-powered portable electronic micro-devices, such as structure-embedded monitoring systems, biomedical implants, and ad-hoc wireless transceiver micro-sensors, continue to incorporate increasingly more functions into smaller form-factors. Even with improved power-efficient designs, low duty-cycle task multiplexing, and smart power-aware networks, the energy stored in micro-scale batteries (e.g., thin-film lithium-ion batteries – Li-Ion [1]) is not sufficient to sustain extended lifetimes [2]. Long-lasting, self-renewable, chip-compatible *in situ* energy harvesting sources are therefore the subject of research for a growing number of engineers and scientists, especially as it pertains to self-sustaining, self-powered, micro-scale, system-in-package (SiP) applications.

Ambient solar [3], kinetic (vibrations) [4-5], and thermal [6] energy can be harnessed on-chip with photovoltaic cells and micro-electromechanical systems (MEMS) generators. The amounts of energy and power levels that can be achieved, however, depend on the conditions surrounding the application and the compatibility of the available technologies [7]. Mobile and outdoors applications, for instance, are more likely to vibrate and be exposed to useful solar energy levels. The likelihood of exposing a micro-system to large thermal gradients, on the other hand, tends to be low. Mechanical vibrations from engines, flowing water, gusting winds, moving people, and so on are in fact more likely and consequently more abundant, stable, and predictable [4].

Energy from ambient mechanical vibrations can be harvested by means of a magnetic field [8], electric field [9-12], or strain on a piezoelectric material [13]. Electromagnetic and piezoelectric scavengers, however, are less CMOS-compatible and less scalable. Fortunately, electrostatic harvesters are fully compatible with MEMS technologies and capable of generating moderate power levels

without the use of exotic materials or obscure process steps. It is for these reasons that the proposed system scavenges kinetic energy with an electrostatic harvester and stores it in a thin-film Li-Ion polymer battery, as shown in Fig. 1, from which power is distributed based on the functional demands of the application.

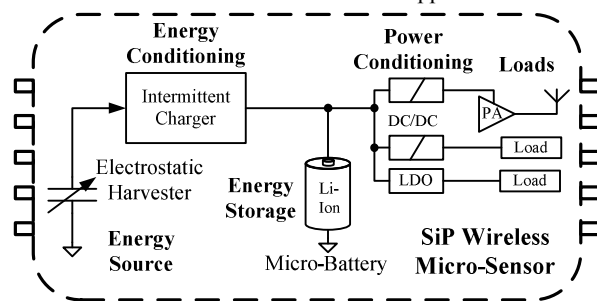


Figure 1. System-in-package (SiP) wireless micro-sensor.

## II. HARVESTING ELECTROSTATIC ENERGY

An electrostatic energy scavenger harnesses energy from the work done by vibrations against an electric field, the embodiment of which relies on the changing capacitance of a vibration-dependant MEMS variable plate capacitor. Mechanical energy is converted into electrical energy as the plates of the charged capacitor separate in response to externally applied vibrations, while either voltage or charge is constrained [9]. The capacitor must be pre-charged at its maximum capacitance point (i.e., minimum plate separation) before energy can be harvested. The pre-charge energy is required to initiate the harvesting cycle, much like the energy a lead-acid battery invests in initially turning a car engine. This initial investment must of course constitute only a fraction of the net energy gained.

### A. Charge-Constrained Harvesting

In a charge-constrained scheme, charge is held constant by open-circuiting a capacitor as its plates separate in response to vibrations. This decrease in capacitance causes the voltage across the device to necessarily increase ( $Q_{\text{Constant}} = C_{\text{MEMS}}V$ ) and, since the relation between voltage and capacitor energy is squared rather than linear, as is with capacitance ( $E_C = \frac{1}{2}C_{\text{MEMS}}V^2$ ), the net energy stored in the capacitor increases. The main drawback to this technique, however, is that the magnitude of the increasing voltage surpasses the breakdown limits of most modern CMOS technologies. For instance, a 100-to-1 pF variation produces a 2.7-to-270 V change across the capacitor, assuming an initial voltage of only 2.7 V, which is the low voltage limit of a standard Li-Ion battery. Specialized silicon-on-insulator (SOI) process technologies can sustain these voltages [11] but they are not compatible with standard CMOS process nodes and therefore not conducive toward system integration of micro-scale systems.

### B. Voltage-Constrained Harvesting

In the voltage-constrained method, the voltage across the capacitor is held constant through the harvesting phase, when the parallel-plate distance increases and capacitance decreases, which drives charge out of the capacitor ( $Q = C_{\text{MEMS}}V_{\text{Constant}}$ ). The me-

chanical energy required to move the plates and charges is therefore harvested and stored in another capacitor or, better yet, a rechargeable battery. The variable capacitor behaves like a current source because the change in capacitance causes variations in charge, in spite of no changes in voltage,

$$\dot{q} = \frac{dQ}{dt} = C \frac{\partial V}{\partial t} + V \frac{\partial C}{\partial t} = V \frac{\partial C}{\partial t}, \quad (1)$$

all of which is entirely controlled and energized by vibrations.

Maintaining the voltage across the capacitor constant requires a voltage source [9] or an electret material [12]. In the proposed system, however, the MEMS capacitor is directly connected to the energy storage device during the harvesting phase, which in this case is a Li-Ion battery. As a result, pre-charging this variable capacitor to the battery voltage and connecting it to the Li-Ion battery ensures the voltage across the MEMS capacitor remains constant (at the battery voltage) throughout the harvesting cycle.

### III. PROPOSED VOLTAGE-CONSTRAINED SCHEME

In the proposed scheme, the energy harvester operates in three separate phases: pre-charge, harvesting, and recovery (Fig. 2). The variable capacitor is first pre-charged to the battery voltage via a quasi-lossless energy transfer circuit. Before the onset of the harvesting phase, the MEMS capacitor is connected to the battery through a switch; and since both are at the same voltage, no power is dissipated in the switch. During harvesting, when the capacitor plates separate and capacitance decreases, charge flows into the battery and energy is harvested and stored. When the capacitor reaches its minimum value, the energy left in the capacitor is restored and driven back to the battery.

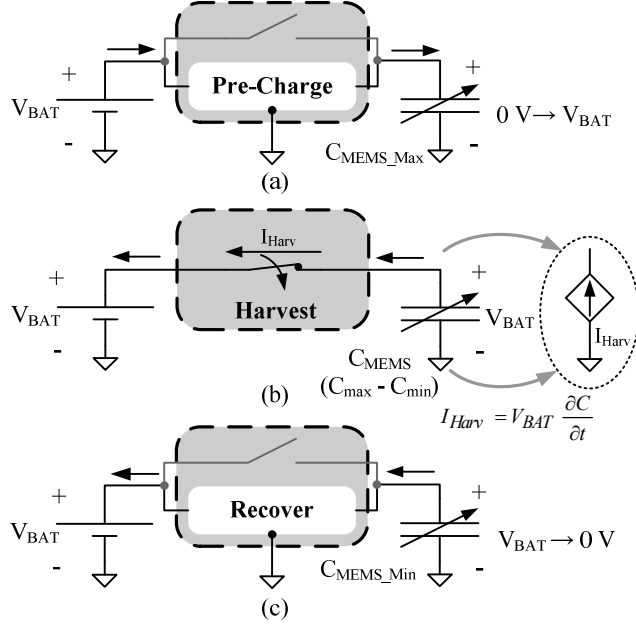


Figure 2. (a) Pre-charge, (b) harvesting, and (c) recovery phases of the proposed voltage constrained, energy-harvesting scheme.

For the system to yield a net gain, energy harvested and recovered must exceed the energy invested in the system. Assuming energy is transferred without any power losses, the initial investment needed to pre-charge the capacitor and initiate the process is

$$\Delta E_{\text{Invested}} = \frac{1}{2} C_{\text{Max}} V_{\text{Bat}}^2. \quad (2)$$

The energy stored in the battery during the harvesting phase is

$$\Delta E_{\text{Harvested}} = \int V_{\text{Bat}} i_{\text{Harv}}(t) dt = V_{\text{Bat}}^2 \int \frac{dC(t)}{dt} dt = V_{\text{Bat}}^2 \Delta C. \quad (3)$$

To complete the cycle, after the minimum capacitance is reached and harvesting ends, the energy remaining in the capacitor is recovered with the same quasi-lossless block used in the pre-charge phase (Fig. 2(c)),

$$\Delta E_{\text{Recovered}} = \frac{1}{2} C_{\text{Min}} V_{\text{Bat}}^2. \quad (4)$$

Again, assuming power losses during the various transitions are negligible, the net energy gain of the system is

$$\Delta E_{\text{Net}} = -\Delta E_{\text{Invested}} + \Delta E_{\text{Harvested}} + \Delta E_{\text{Recovered}} = \frac{1}{2} \Delta C V_{\text{Bat}}^2. \quad (5)$$

Once the energy is recovered and the capacitor is fully discharged, there is no electric field and the capacitor plates are therefore free to move and return to their original minimum separation state without requiring any electrical energy. However, power losses are not negligible, and a more accurate description of the net energy gain is

$$\Delta E_{\text{Net}} = \frac{1}{2} \Delta C V_{\text{Bat}}^2 - \sum P_{\text{Losses}} T_{\text{Vib}}, \quad (6)$$

where  $P_{\text{Losses}}$  represents the various average power loss components of the system, which are discussed in a latter section.

### IV. PROPOSED HARVESTER CIRCUIT

#### A. Harvesting

Key to the success of the harvester is transferring energy without incurring significant power losses, which is why an inductor-based circuit is proposed, as illustrated in Fig. 3. The pre-charge phase is therefore decomposed into a sequence of two steps. First, energy is transferred from the Li-Ion battery into the inductor by superimposing the battery voltage across the inductor with switches  $S_1$  and  $S_3$  (Step 1). The inductor current then increases linearly, and when sufficient energy is stored,  $S_1$  and  $S_3$  open. The second step is to drive the stored energy into the variable MEMS capacitor by connecting the inductor to the capacitor with  $S_2$  and  $S_4$  (Step 2). The inductor current ultimately charges the variable capacitor until its voltage reaches that of the battery, at which point  $S_2$  and  $S_4$  open.

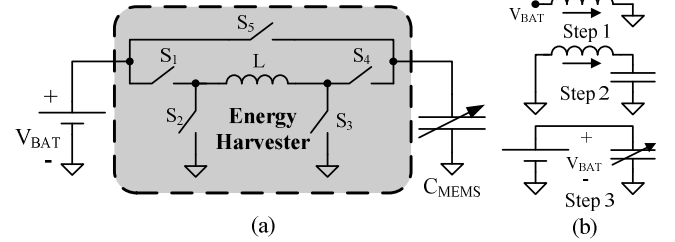


Figure 3. (a) Proposed energy harvesting system and (b) the connectivity of the various charge-discharge cycles.

During the harvesting phase, the MEMS capacitor is connected to the rechargeable battery with  $S_5$  (Step 3) so that charge can be driven into the battery. Since the battery is a low impedance source, the voltage across the battery is for all practical purposes constant and the decreasing capacitance therefore produces a harvesting current. Although this current charges the battery, the resulting increase in voltage is minimal because the magnitude of the current is low, which is why the capacitor voltage is said to be constrained.

After harvesting ends, the energy left in the capacitor is a small fraction of the total energy harvested and not worth recovering, when considering circuit complexity and power losses. In the proposed scheme, this energy constitutes a negligible loss. Consequently, after opening all the switches, the capacitor is allowed to return to its minimum plate separation state under charge-

constrained conditions, thereby decreasing the capacitor voltage to approximately 0 V.

### B. Circuit

The harvesting circuit is comprised of a rechargeable Li-Ion battery, a MEMS variable capacitor, the proposed inductor-based harvester circuit, and a control signal generator, as shown in Fig. 4. The battery is modeled with a large capacitor in series with an equivalent series resistance (ESR) [14] and its capacitance is a measure of the maximum capacity available in the battery – a thin-film Li-Ion polymer battery can have up to 100  $\mu\text{Ah}/\text{cm}^2$  [15]. The voltage across the battery can vary from 2.7 V, when it is fully discharged, to its fully charged state of 4.2 V.

In response to mechanical vibrations, The MEMS variable capacitor decreases from 100 to 1 pF. Its model includes a varactor and a 1 pF parasitic capacitor with its own ESR. To simplify simulations and prove functionality, the capacitance variance is assumed to be linear with time and much longer in duration than the pre-charge phase. For the sample signals shown in Fig. 4, the maximum-to-minimum change occurs within 10  $\mu\text{s}$  of a 15  $\mu\text{s}$  vibration period, and because the capacitance changes linearly under a constant 4 V battery voltage, a constant harvesting current of approximately 40  $\mu\text{A}$  is produced ( $4\text{ V} \cdot 100\text{ pF} / 10\text{ }\mu\text{s}$ ).

The pre-charge circuitry features a 1  $\mu\text{H}$  inductor and its ESR; CMOS switches  $\text{MP}_1$ ,  $\text{MN}_2$ , and  $\text{MN}_3$ ; a CMOS transmission gate comprised of  $\text{MN}_4$  and  $\text{MP}_4$ ; and all relevant parasitic body diodes. The inductor is charged when transistors  $\text{MP}_1$  and  $\text{MN}_3$  are ON, and conversely, discharged into MEMS capacitor  $C_{\text{MEMS}}$  when transistors  $\text{MN}_2$ ,  $\text{MP}_4$ , and  $\text{MN}_4$  are ON.  $\text{MN}_4$  is added because  $\text{MP}_4$  is exhausted of gate-drive when  $C_{\text{MEMS}}$  is initially discharged, which is initially the case during the pre-charge phase. To pre-charge  $C_{\text{MEMS}}$  (100 pF) to  $V_{\text{Bat}}$  (4 V), at least 800 pJ must be transferred from the battery, generating a peak inductor current of roughly 40 mA. Smaller inductance values would result in higher currents, but the corresponding larger switches would compromise integration.

The control signals necessary to operate the harvester circuit are generated by a low-power digital-signal processing (DSP) block. During pre-charge, signal  $\Phi_{\text{L-Charge}}$  goes high to close switches  $\text{MP}_1$  and  $\text{MN}_3$  and energize the inductor. After a pre-determined charging time, the switches are opened and a dead-time (all switches are OFF) is inserted. Dead-time is included between every switching transition to prevent short-circuit conditions and large peaking volt-

ages. Signal  $\Phi_{\text{L-Discharge}}$  then goes high to close switches  $\text{MN}_2$ ,  $\text{MN}_4$ , and  $\text{MP}_4$  and charge  $C_{\text{MEMS}}$ . When the capacitor voltage reaches the battery voltage, pre-charge ends and signal  $\Phi_{\text{L-Discharge}}$  is returned to its low state. After another dead-time, signal  $\Phi_{\text{Harvest}}$  closes switches  $\text{MP}_{5A}$  and  $\text{MP}_{5B}$  and starts the harvesting phase.  $\text{MP}_{5A}$  and  $\text{MP}_{5B}$  effectively constitute one switch but they were implemented separately to ensure their parasitic body diodes do not discharge  $C_{\text{MEMS}}$  during the pre-charge phase, which is achieved by connecting their respective body diodes back-to-back.

### C. Power Losses

*Pre-Charge Phase:* Resistances and body diodes determine the conduction power losses of the pre-charge phase. The cumulative ESR of the capacitor, inductor, and battery; the channel impedances of the various switches; and the triangular inductor current flowing through them (Fig. 4) result in resistive power losses,

$$P_{\text{Cond}} = I_{\text{L,RMS}}^2 R_{\text{eq}} \tau_{\text{Cond}} f_{\text{Vib}}, \quad (7)$$

where  $P_{\text{Cond}}$  is averaged over time,  $I_{\text{L,RMS}}$  is the root-mean square (RMS) value of the inductor current,  $R_{\text{eq}}$  the equivalent resistance of the circuit path in question,  $\tau_{\text{Cond}}$  the total conduction time, and  $f_{\text{Vib}}$  the vibration frequency.  $I_{\text{L,RMS}}$  always flows through  $R_{\text{ESR,L}}$ , two MOS switches, and one of two other ESRs: (1) when storing current in L,  $R_{\text{ESR,BAT}}$ ,  $R_{\text{ds,MP1}}$ ,  $R_{\text{ESR,L}}$ , and  $R_{\text{ds,MN3}}$ ; and (2) when delivering current to  $C_{\text{MEMS}}$ ,  $R_{\text{ds,MN3}}$ ,  $R_{\text{ESR,L}}$ ,  $R_{\text{ds,MN4-MP4}}$ , and  $R_{\text{ESR,MEMS}}$ .

$$P_{\text{Cond}} \approx N \left( I_{\text{L,Max}}^2 \right) \left( 2R_{\text{ds}} + R_{\text{ESR,L}} + R_{\text{ESR,BC}} \right) \tau_{\text{L}} f_{\text{Vib}}, \quad (8)$$

where  $N$  is the number of inductor storage-delivery cycles within the pre-charge phase,  $I_{\text{L,Max}}$  the peak inductor current,  $\tau_{\text{L}}$  the storage time of one cycle (which is approximately also equal to delivery time),  $R_{\text{ESR,BC}}$  represents the ESR of the battery and  $C_{\text{MEMS}}$ , and the parallel resistance of  $\text{MN}_4$ - $\text{MP}_4$  is depicted as a single equivalent  $R_{\text{ds}}$  for simplicity. During the dead time inserted between the current storage and delivery cycles, current flows through the body diodes of  $\text{MN}_2$  and  $\text{MP}_4$ ,  $R_{\text{ESR,L}}$ , and  $R_{\text{ESR,MEMS}}$ , incurring additional conduction power losses:

$$P_{\text{Dead}} = N \left[ I_{\text{L,Max}}^2 \left( R_{\text{ESR,L}} + R_{\text{ESR,MEMS}} \right) + 2I_{\text{L,Max}} V_{\text{Diode}} \right] \tau_{\text{Dead}} f_{\text{Vib}}, \quad (9)$$

where the dead current is  $I_{\text{L,Max}}$ ,  $V_{\text{Diode}}$  is the voltage drop across each body diode, and  $\tau_{\text{Dead}}$  is the dead time.

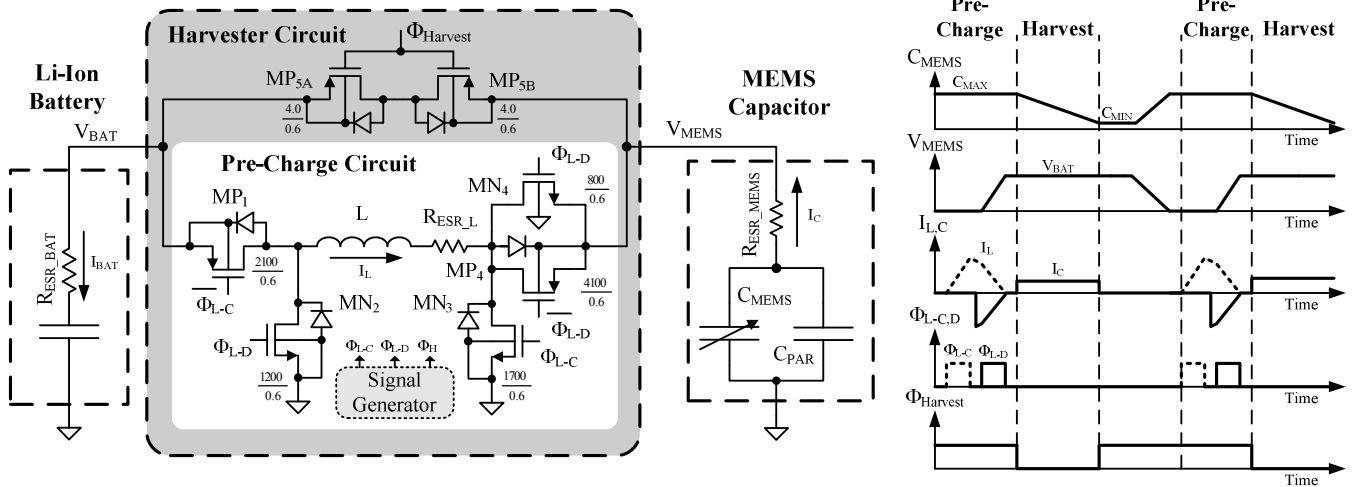


Figure 4. Complete energy harvester circuit with Li-Ion battery, MEMS variable capacitor, and various control signals.

The control electronics must charge and discharge all stray MOS capacitors, dissipating in the process switching power losses, which include I-V overlap and gate-drive losses [16]. To reduce these parasitic effects, small area and therefore short gate-length transistors are adopted. Since gate-widths determine the effective channel resistances of the switches, their values represent a compromise between conduction and switching losses. In the proposed circuit, the average I-V overlap power lost per switch is

$$P_{I-V} = N \left( \frac{1}{2} V_{\text{Peak}}^2 \right) C_{d,\text{Par}} f_{\text{Vib}}, \quad (10)$$

where  $V_{\text{Peak}}$  is the drain-source voltage of the switch before turning ON and  $C_{d,\text{Par}}$  represents the total parasitic capacitance at the transistor drain. The OFF drain-source voltage of  $MP_1$  and  $MN_2$  is approximately equal to the battery voltage; however, the initial drain-source voltage across transistors  $MN_3$ ,  $MN_4$ , and  $MP_4$ , when turned ON, is close to zero since the capacitor is fully discharged. Therefore, these transistors operate in zero voltage switching (ZVS) conditions and their switching losses are considerably low [17]. As a result, the size of these transistors can be increased to reduce resistive power losses without sacrificing I-V overlap losses in the process. The assumption is no longer valid when more than one inductor charge-discharge cycle is adopted because the capacitor will have an initial voltage across it after the first cycle.

Gate-drive power losses refer to the energy required to charge and discharge parasitic capacitors present at the transistor gate. The average power lost per switching event (turn-ON or OFF) is

$$P_{\text{GDrive}} = \frac{1}{2} N C_{g,\text{Par}} V_{\text{Drive}}^2 f_{\text{Vib}}, \quad (11)$$

where  $C_{g,\text{Par}}$  is the equivalent parasitic capacitance at the device gate and  $V_{\text{Drive}}$  is the drive voltage, which in this case is approximately equal to the battery voltage. These driving losses are incurred by the driving stage within the DSP block.

**Harvesting Phase:** When the system is harvesting energy, only transistors  $MP_{5A}$  and  $MP_{5B}$  interact directly with the harvesting current. The transistors are sized so that their parasitic capacitances do not create charge leakage problems. However, their cumulative channel resistance ( $R_{\text{ds5}}$ ) is relatively larger and the resulting conductive power loss is

$$P_{\text{Harv\_Cond}} = I_{\text{Harv}}^2 (R_{\text{ds5}} + R_{\text{ESR\_MEMS}} + R_{\text{ESR\_BAT}}) \tau_{\text{Max-Min}} f_{\text{Vib}}, \quad (12)$$

where  $I_{\text{Harv}}$  is the harvesting current, and  $\tau_{\text{Max-Min}}$  represents the time it takes the capacitor to reach its minimum capacitance point. However, the voltage drop across the equivalent path resistance will increase the voltage across the capacitor, effectively increasing the harvesting current (and energy). As a result, the power dissipated in this resistance is provided by extra mechanical work performed by the MEMS device and not from the battery or the electrical energy generated. This additional energy is offset by adjusting the elasticity of the variable MEMS capacitor, the physical design of which is beyond the scope of this paper.

**Voltage Mismatch Loss:** In a practical solution, a voltage mismatch will exist between the pre-charged  $C_{\text{MEMS}}$  and the battery, and when connected through harvesting switch  $MP_{5A-B}$ , energy is exchanged and conduction losses result by way of switch resistance. This power loss is approximately

$$P_{\text{Mismatch}} = \frac{1}{2} C_{\text{Max}} V_{\text{Mismatch}}^2 f_{\text{Vib}}, \quad (13)$$

where  $V_{\text{Mismatch}}$  represents the difference in voltages between the battery and  $C_{\text{MEMS}}$  after the pre-charge phase. Overcharging the capacitor during the pre-charge phase (i.e.,  $V_{\text{CMEMS}} > V_{\text{BAT}}$ ) incurs lower power losses than undercharging it because the pre-charge circuit is quasi lossless and the harvesting switch is not, and part of the additional charge flows back to the battery. That is to say, charging through a lossless circuit is better than through a lossy

switch, not to mention that part of the additional energy transferred to  $C_{\text{MEMS}}$  is ultimately recovered by the battery at the onset of the harvesting phase.

## V. SIMULATION RESULTS

The proposed harvester was simulated with TSMC's 0.35  $\mu\text{m}$  technology BSIM3 transistor models and a behavioral Analog-HDL MEMS capacitor model. As previously noted, the recovery phase was omitted because the residual energy left in  $C_{\text{MEMS}}$  after the harvesting phase is impractically low. The ESRs of the battery and capacitor are assumed to be near 100 m $\Omega$  and the inductor ESR around 750 m $\Omega$  [18]. The Li-Ion battery voltage is assumed to be near 4 V, that is to say, neither fully charged nor discharged.

As shown in Fig. 5, the capacitor voltage was pre-charged to 4.269 V, 7% above the battery voltage. Approximately 136 pJ of this additional energy investment was delivered back to the battery during the harvesting phase, through harvesting switch  $MP_{5A-B}$ , as a result of voltage mismatch. A single storage-delivery cycle was used to pre-charge the capacitor to this voltage level and its peak inductor current was 45.9 mA. In the end, the energy invested and lost during this phase was about 1.15 nJ.

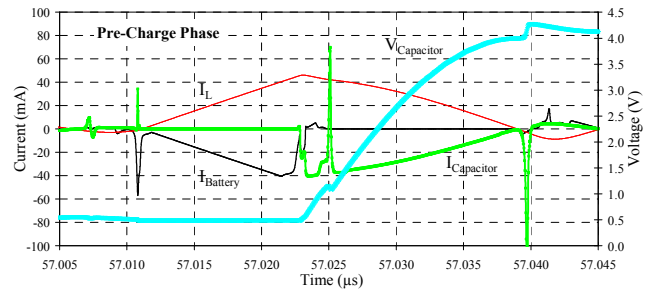


Figure 5. Current waveforms and capacitor voltage during pre-charge.

During the harvesting phase, as capacitance decreases, a 40.8  $\mu\text{A}$  harvesting current is generated and its value is for the most part constant, except for the initial RC response seen in Fig. 6, which is produced by the channel resistance of  $MP_{5A-B}$  in series with  $C_{\text{MEMS}}$ . Each harvesting cycle harnesses approximately 1.58 nJ. The net energy of the battery increases linearly at a rate of 569 pJ per cycle, as shown in Fig. 7 and summarized in Table I, the net result of which is an average power gain of 38  $\mu\text{W}$ . Comparing it with the maximum theoretical energy gain of 792 pJ (Eq. 5) and assuming 100% mechanical-to-electrical energy conversion, the efficiency (actual-to-theoretical energy-gain ratio) of the harvester is approximately 71.8% (i.e., 71.8% of 792 pJ was harvested).

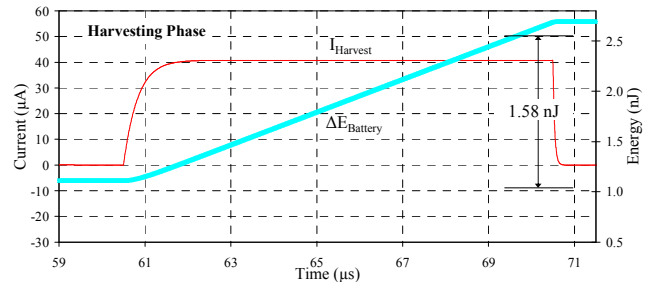


Figure 6. Battery current and energy during the harvesting phase.

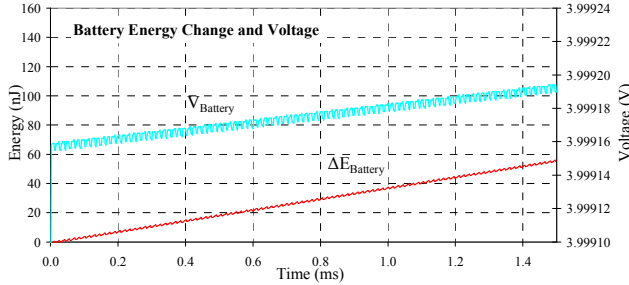


Figure 7. Steady-state battery voltage and energy change under constant vibration (i.e., frequency is constant).

TABLE I. POWER BUDGET

Power Component	Power	Energy per Cycle
<b>Pre-Charge Phase</b>		
$P_{Losses} = P_{Cond} + P_{I,V} + P_{Dead}$	15.23 $\mu$ W	228.4 pJ
$P_{Invested}$ (Energy in capacitor)	61.35 $\mu$ W	920.3 pJ
$P_{Pre-Charge} = P_{Losses} + P_{Invested}$	<b>76.58 <math>\mu</math>W</b>	<b>1148.7 pJ</b>
<b>Returned Over-Charge Energy</b>		
$P_{Return}$	<b>9.08 <math>\mu</math>W</b>	<b>136.23 pJ</b>
<b>Harvesting Phase</b>		
$P_{Harvest}$	<b>105.43 <math>\mu</math>W</b>	<b>1581.4 pJ</b>
<b>Net Power Gain</b>		
$P_{Net} = P_{Harvest} + P_{Return} - P_{Pre-Charge}$	<b>37.93 <math>\mu</math>W</b>	<b>568.95 pJ</b>

## VI. DISCUSSION

The aforementioned results show that energy can be harvested from a variable plate capacitor and stored into a micro-Li-Ion battery. The working assumption is that vibrations are synchronous, in other words, cyclic and periodic. This is indeed the case for engines, turbines, a heartbeat, and others, for which the harvester can be precisely designed and synchronized. However, asynchronous applications like human (or animal) movement require self-adapting schemes. These systems must sense the change in capacitance directly or indirectly and synchronize the system to its peaks and valleys, or adopt an asynchronous approach [11], where the capacitor plates separate only with sufficiently large accelerations. These requirements, however, are circumvented in synchronous applications, for which the work presented in this paper is targeted.

To simplify the derivations,  $C_{MEMS}$  is assumed to change linearly with time, and this may not necessarily be the case. Nevertheless, all that is needed to harvest energy is a net change in capacitance. Having the capacitance non-monotonically decrease does incur additional conduction losses through the harvesting switch, as current momentarily reverses direction and non-losslessly charges  $C_{MEMS}$ , partially offsetting the lossless character of the pre-charge circuit. In practice, however, capacitance is expected to vary monotonically in the presence of synchronous vibrations, thereby avoiding these current reversal events and their associated power losses.

## VII. CONCLUSION

An electrostatic energy harvesting micro-system was presented and evaluated. It was able to harness approximately 570 pJ per cycle in the presence of vibrations with a period of 15  $\mu$ s, resulting in a net average power supply of 38  $\mu$ W. The mechanical energy exerted by the environment to move the two capacitor plates apart against an electric field was effectively converted into a harvesting current of 40.8  $\mu$ A. A thin-film polymer Li-Ion battery is not only used to store the energy harvested and clamp the capacitor voltage during the voltage-constrained harvesting cycle but also to jump-start the system by pre-charging the capacitor during start-up. The

foregoing assumptions were synchronous vibrations and monotonic capacitance variations, both of which are the case in engines and other synchronous applications. Given the magnitude of the energy levels harvested, all control circuits must consume only a fraction of the total energy harvested. Digital and sub-threshold analog designs are therefore attractive. Circuits must also be managed to activate only when necessary. In all, the harvester solution proposed is capable of replenishing energy that is consumed by the system and therefore able to power a self-sustaining micro-scale system like a wireless system-in-package (SiP) micro-sensor, indefinitely extending its operational life.

## REFERENCES

- [1] J.B. Bates, N.J. Dudney, B. Neudecker, A. Ueda, and C.D. Evans, "Thin-film lithium and lithium-ion batteries," *Solid State Ionics*, vol. 135, pp. 33-45, 2000.
- [2] D. Puccinelli and M. Haenggi, "Wireless sensor networks: applications and challenges of ubiquitous sensing," *IEEE Circuits and Systems Magazine*, vol. 3, no. 3, pp. 19-29, 2005.
- [3] B.A. Warneke, M.D. Scott, B.S. Leibowitz, L. Zhou, C.L. Bellew, J.A. Chediak, J.M. Kahn, B.E. Boser, and K.S. Pister, "An autonomous 16 mm<sup>3</sup> solar-powered node for distributed wireless sensor networks," *Proceedings of IEEE Sensors*, pp. 1510-5, 2002.
- [4] S. Roundy, P. Wright, and J. Rabaey, "A study of low level vibrations as a power source for wireless sensor nodes," *Computer Communications*, vol. 26, pp. 1131-44, 2003.
- [5] P.D. Mitcheson, T.C. Green, E.M. Yeatman, and A.S. Holmes, "Architectures for vibration-driven micropower generators," *IEEE Journal of Microelectromechanical Systems (MEMS)*, vol. 13, pp. 429-440, 2004.
- [6] M. Stordeur and I. Stark, "Low power thermoelectric generator – self-sufficient energy supply for micro systems," *16<sup>th</sup> International Conference on Thermoelectrics*, pp. 575-7, 1997.
- [7] E.O. Torres and G.A. Rincón-Mora, "Long-lasting, self-sustaining, and energy-harvesting system-in-package (SiP) wireless micro-sensor solution," *International Conference on Energy, Environment, and Disasters (INCEED)*, Charlotte, NC, 2005.
- [8] H. Kula and K. Najafi, "An electromagnetic micro power generator for low-frequency environmental vibrations," *Proc. 17<sup>th</sup> IEEE Conf. on Micro Electro Mechanical Systems (MEMS)*, 2004, pp. 237-240.
- [9] S. Meninger, J. Mur-Miranda, R. Amirtharajah, A. Chandrakasan, and J. Lang, "Vibration-to-electric energy conversion," *IEEE Transactions On Very Large Scale Integration (VLSI) Systems*, vol. 9, pp. 64-76, 2001.
- [10] P.D. Mitcheson, P. Miao, B.H. Stark, E.M. Yeatman, A.S. Holmes, and T.C. Green, "MEMS electrostatic micropower generator for low frequency operation," *Sensors and Actuators A*, vol. 115, pp. 523-529, 2004.
- [11] B.H. Stark, P.D. Mitcheson, P. Miao, T.C. Green, E.M. Yeatman, and A.S. Holmes, "Converter circuit design, semiconductor device selection and analysis of parasitics for micropower electrostatic generators," *IEEE Transactions on Power Electronics*, vol. 21, no. 1, pp. 27-37, 2006.
- [12] T. Sterken, P. Fiorini, K. Baert, R. Puers, and G. Borghs, "An electret-based electrostatic  $\mu$ -generator," *12<sup>th</sup> International Conference on Solid State Sensors, Actuators, and Microsystems*, Boston, MA, pp. 1291-4, 2003.
- [13] S. Roundy and P.K. Wright, "A piezoelectric vibration based generator for wireless electronics," *Smart Materials and Structures*, vol. 13, pp. 1131-1142, 2004.
- [14] J. Formenti and R. Martinez, "Design trade-offs for switch-mode battery chargers," *Texas Instruments Portable Power Design Seminar*, 2004.
- [15] D. Linden and T.B. Reddy, *Handbook of Batteries*, 3<sup>rd</sup> ed., New York: McGraw-Hill, ch. 35, 2002.
- [16] L. Balogh, "Design and application guide for high speed MOSFET gate drive circuits," *Texas Instruments Power Supply Design Seminar (SEM-1400)*, 2001.
- [17] M. Gildersleeve, H.P. Forghani-zadeh, and G.A. Rincón-Mora, "A comprehensive power analysis and a highly efficient, mode-hopping dc-dc converter," *IEEE Asia-Pacific Conference on ASICs*, pp. 153-6, Taipei, Taiwan, 2002.
- [18] S. Musunuri, P.L. Chapman, J. Zou, and C. Liu, "Design issues for monolithic dc-dc converters," *IEEE Transactions on Power Electronics*, vol. 20, no. 3, pp. 639-49, 2005.